





Perceptually Guided Automatic Parameter Optimization for Interactive Visualization

D. Opitz^{1,2} , T. Zirr^{1,2} , C. Dachsbacher¹ , L. Tessari² 

¹Karlsruhe Institute of Technology
²Intel Corporation

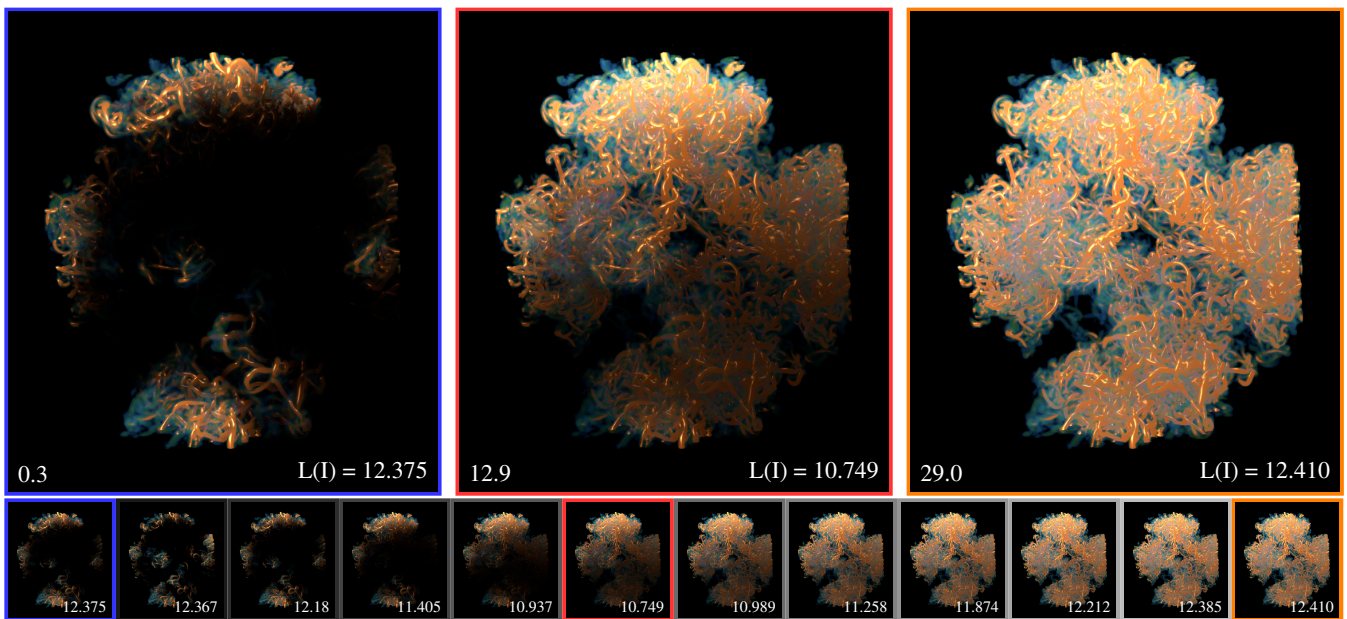


Figure 1: This example shows a time-dependent Vortex Cascade dataset rendered with low-pass filtered volumetric shadows (LPFV) [ASDW14]. The shadow's softness, is adjusted with a single parameter – the filter kernel size (number in the bottom left). The proposed model computes a perceived loss of information in the image $L(I)$ (number in the bottom right). The bottom sequence shows images rendered with an increasing softness of the volumetric shadows for comparison. We use an automatic parameter search to find the optimal parameter used for the center top image. Note that all images are intended to be displayed to a standard observer, see section Sect. 4.1 for details.

Abstract

We propose a new reference-free method for automatically optimizing the parameters of visualization techniques such that the perception of visual structures is improved. Manual tuning may require domain knowledge not only in the field of the analyzed data, but also deep knowledge of the visualization techniques, and thus often becomes challenging as the number of parameters that impact the result grows. To avoid this laborious and difficult task, we first derive an image metric that models the loss of perceived information in the processing of a displayed image by a human observer; good visualization parameters minimize this metric. Our model is loosely based on quantitative studies in the fields of perception and biology covering visual masking, photo receptor sensitivity, and local adaptation. We then pair our metric with a generic parameter tuning algorithm to arrive at an automatic optimization method that is oblivious to the concrete relationship between parameter sets and visualization. We demonstrate our method for several volume visualization techniques, where visual clutter, visibility of features, and illumination are often hard to balance. Since the metric can be efficiently computed using image transformations, it can be applied to many visualization techniques and problem settings in a unified manner, including continuous optimization during interactive visual exploration. We also evaluate the effectiveness of our approach in a user study that validates the improved perception of visual features in results optimized using our model of perception.

1. Introduction

In the last decades numerous visualization techniques have been developed ranging from methods tailored for very specific problems to more general approaches. Typically, these techniques all define their own set of parameters which need to be chosen or adjusted to obtain an image that best conveys the essential information from the visualization data. However, determining an optimal or at least well-working set of parameters is often non-trivial. For example parameter settings might depend on the input data, like the presence of certain features, or scale. In addition, a user performing a visualization task could be an expert in the application domain, but might not be aware of the inner workings of parameters that control the visualization itself. Sometimes tuning parameters is challenging even for visualization experts: When an image is presented to the human visual system, the perception of one stimulus may affect the presence of another leading to visual masking. This is just one example of difficulties that arise as a result of the complex interplay of features in data sets, transparency, illumination, and shading. Moreover, different viewing conditions might affect the quality of previously tested parameters, causing unexpected loss of visual information.

In this paper, we present a novel method for automatically choosing and optimizing parameters for visualization techniques without requiring user interaction. Our method is purely image-based and thus agnostic to the visualization technique or semantics of its parameters: we develop a perception-based model and corresponding metric to quantify the loss of perceived information in the human visual system when a user observes an image on the screen. The model is built on quantitative findings in the fields of perception and biology and utilizes established information theory operations. It enables us to automatically search for visualization parameters which minimize this loss and thus increase the visualized information. In summary, our contributions in this paper are:

- We devise a model and corresponding metric to quantify the perceived information relative to the displayed image and thus the loss of information we seek to minimize.
- We show how this metric can be used to determine a set of well-working parameters for a visualization and allows for background optimization of the parameters during interactive visualization.
- We demonstrate the quality of our method predominantly for direct volume rendering which provides several parameters to control the visualization.
- We conduct a user study to verify the validity of our model of the human visual system and perceptual loss metric.

Note that we distance our proposed approach from techniques that look directly at the data set and apply some form of preprocessing e.g. filtering or highlighting regions. Instead, we focus on reducing visual artifacts in the rendered image, making this work immediately embeddable in any visualization framework. Considering the image-based nature of our approach, we use the term visualization technique to generally describe the mapping of a scientific dataset to a 2D image.

In [Sect. 2](#) we present previous work related to this paper. [Sect. 3](#) describes our method in detail. In [Sect. 4](#) we present and discuss the results of our method when applied to different visualization scenarios. [Sect. 5](#) concludes the paper with future work.

2. Previous Work

In this section we discuss previous work on optimization of visualization tasks, as well as on information theory and perception in the context of visualization upon which our method is based on. For a broader overview, Wang et al. [[WS11](#)] provide a comprehensive introduction to information theory in visualization, and the surveys by Tory et al. [[TM04](#)], and Haeley et al. [[HE12](#)] give a thorough introduction into perceptual aspects.

Optimization of Visualization Tasks Getting the best possible results of a visualization has been the focus of many works. Jänkicke et al. use saliency [[JC10](#)], while Bramon et al. use information theoretic principles [[BRB*13](#)] to evaluate visualizations of volume data. Enhancing the visualization of flow by selecting streamlines and viewpositions [[TMWS13](#)], finding good streamline seeds [[XLS10](#)], or evaluating the carried information by line segment lengths [[FI08](#)] and curvature [[MCHM10](#)] of streamlines. Behrisch et al. [[BBK*18](#)] provide an extensive survey concerning quality metrics that may be used for different plots and types of information visualization.

Information Theory in Visualization Information theory is the basis for many existing methods in computer graphics, and entropy-based methods are used in the field of computer vision. Entropy-based image processing has been applied to image segmentation [[TTL03, dAEMdA04](#)], classification [[JM04](#)], and object recognition [[KON02, LSP05](#)]. There are many visualization-specific applications of information theory, of which we will give a short overview in the following.

Image Quality Metrics The Visual Difference Predictor [[Dal92](#)] is a mathematical model that assesses the image fidelity, the equivalence of two images under certain display parameters and viewing conditions, implemented as a sequence of image processes. Similarly, the Visual Discrimination Model by Lubin [[Lub95](#)] predicts the visual discriminability of images with a perceptual model. Saghi et al. [[JAS89](#)] present an image quality metric that considers background illumination and spatial frequencies. Visual Embedding [[cDSK*14](#)] provides a more general understanding of the relation between perception and structure in data. For a more in-depth overview of image quality metrics, we refer to [[LJ11](#)].

Perception in Computer Graphics The role of perception for computer graphics by Bartz et al. [[BCFW08](#)] surveys methods that apply insights of human perception to all aspects of computer graphics, rendering, animation, virtual/augmented reality, and visualization. Threshold Maps, introduced by Ramasubramanian et al. [[RPG99](#)], predict a per-pixel threshold for the probability of detecting visual artifacts, and are the base of our perceptual model.

Parameter Selection All rendering techniques are driven by parameters and many different approaches exist to automatically select or manipulate those parameters to approach a suitable result. Lindow et al. [[LBH12](#)] present a method to linearize parameters based on the mean structural similarity index MSSIM. This is a perceptual similarity metric that can be easily converted into a distance measure. They integrate over the parameter space and derive a function that assures a linear change with respect to the used perceptual image

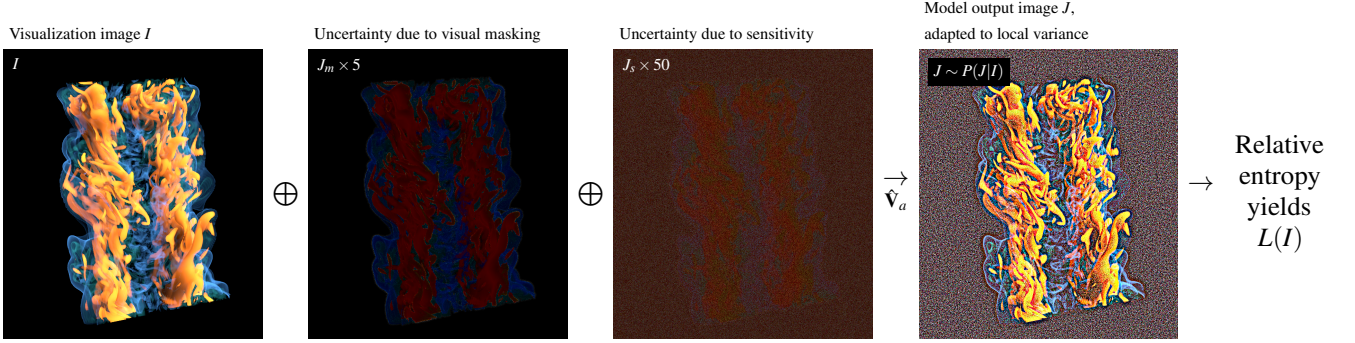


Figure 2: We show the intermediate steps of our model for the perception loss $L(I)$. The left image shows the original image I , a volume rendering of a jet vortex. The center images show the images J_m and J_s , each representing one realization of the distributions P_m for visual masking and P_s for the sensor sensitivity. The distributions are realized by noise proportional to the Threshold Map (Sect. 3.2.1) and the just noticeable difference (Sect. 3.2.2). We obtain the final answer from the human visual system J by performing a contrast enhancement with respect to the observed variance in the image J_{s+m} (Sect. 3.2.3). We obtain a quantitative measure of the information loss due to perception from the relative entropy.

metric. Mindek et al. [MMGB17] extend this concept by guiding the user, reporting back the normalization of the (non-linear) input parameter. Bruckner et al. [BM10] make use of sampling and spatio-temporal clustering techniques, generating an overview of variations in their temporal evolution of physically based simulations for effects. Pineo and Ware [PW12] present a hill climbing algorithm for 2D flow visualizations. Their perceptual model is based on simulating the image processing in the retina and primary visual cortex with a neural network. See Sect. 4.4.2 for a more detailed comparison to our streamline selection example.

3. Method

Visualization techniques are usually controlled by a variety of parameters with diverse effects on the resulting images. Our method strives to find visualization parameters, that minimize the loss of visualized information due to processing by the human visual system (HVS). We drive our optimization with a purely image-based perceptual loss function (Sect. 3.1). This decouples our parameter tuning from the specific underlying visualization technique.

The information loss can be modelled by uncertainties, introduced in the different stages of the HVS (Sect. 3.2), shown in Fig. 2: Visual clutter, for example, introduces uncertainty as a result of visual masking, which can be estimated using Threshold Maps [RPG99]. Noise proportional to the Threshold Map is not noticeable for a human observer, when added to the pixels of an image I . Such uncertainties are undesirable in visualizations as they “waste” precision for displaying useful information. We develop our perceptual model to account for visual masking and sensor sensitivity (adding noise maps J_m and J_s in Fig. 2), and finally contrast sensitivity by modeling local adaptation of the HVS (locally rescaling to obtain J in Fig. 2). Our model provides a distribution of perceptually equivalent images $P(J|I)$ rescaled to fully utilize visual channels, a *model output image* J is a realization of $P(J|I)$.

Finally, we quantify the loss of perception as the statistical distance of the two images J and I . The relative entropy lets us drive an

optimization algorithm, that adapts the current set of visualization parameters (Sect. 3.3) to interactively minimize perceptual uncertainties and thus maximize perceived information. Table 1 summarizes our notation.

| | |
|-------------------------|--|
| I | Displayed visualization image (input) |
| J | <i>Model output image</i> - simulation of processes in the HVS until Visual Cortex, when observing image I |
| $\nabla I, \nabla J$ | Gradient images storing all differences between neighboring pixels (in CIELAB) |
| $P_{\nabla I}(x)$ | Distribution of image gradients for computation of the second-order (relative) entropy |
| $L(I)$ | Perception loss, information lost by human perception |
| $D_{KL}(P \parallel Q)$ | Kullback-Leibler divergence |
| $P(J I)$ | Probability distribution of potential images J registered by a human observing I |
| $P_m(J_m I)$ | Probability distribution modeling masking |
| $P_s(J_s I)$ | Probability distribution modeling sensor sensitivity |
| $I(j), J(j)$ | Pixel value at position j for any images I or respectively J |
| ρ_o | Parameter set being optimized |
| ρ_u | Parameter set fixed by the user |
| ρ_m | Parameters for the perception loss model |
| ρ | Set of all parameters $\rho_o \cup \rho_u \cup \rho_m$ |

Table 1: Notation used throughout the paper.

3.1. Measuring Loss of Visual Information

In order to quantify the information content of images in a way that accounts for spatial structure, we follow the common practice of applying the second-order Shannon entropy [Lar16] to image

data. We are concerned with the change of structural information due to processing by the human visual system (HVS). Therefore, rather than measuring absolute entropy based on the image gradient distribution $P_{\nabla I}(x)$ for an image I , we measure relative entropy by way of comparing the distribution $P_{\nabla I}(x)$ of a displayed image I to the altered distribution $P_{\nabla J}(x)$ of a perceived image J . The Kullback-Leibler divergence [KL51] measures relative entropy in that it quantifies the information lost by representing a distribution $P(x)$ in terms of a distribution $Q(x)$:

$$D_{KL}(P \parallel Q) := \sum_x P(x) \log \frac{P(x)}{Q(x)}. \quad (1)$$

For our purposes, $P(x)$ represents the displayed image I and $Q(x)$ represents the corresponding perceived image J , obtained from our model simulating the HVS. In line with the second-order Shannon entropy, we set $P(x) = P_{\nabla I}(x)$ and $Q(x) = P_{\nabla J}(x)$. Thus, we define our perception loss $L(I)$ as:

$$L(I) := D_{KL}(P_{\nabla I}(x) \parallel P_{\nabla J}(x)). \quad (2)$$

The loss is zero if the distributions $P_{\nabla I}(x)$ and $P_{\nabla J}(x)$ are equal, otherwise it grows with an increasing mismatch between them.

Implementation In order to compute the Kullback-Leibler divergence in practice, we have to settle on a perceptually reasonable approach of computing image gradients for corresponding histograms. We choose the CIELAB color space designed for (locally) perceptual linearity. We construct a gradient histogram by evaluating CIELAB color differences for all eight neighbors of each pixel. Discretized to 6 bits per channel, the differences are aggregated in compact histograms with $6^3 = 262.144$ bins. The Kullback-Leibler divergence is technically undefined for zero valued distributions, i.e. for x with $P_{\nabla I}(x) = 0$. A common solution is to set the corresponding summation term to zero since $\lim_{p \rightarrow 0^+} p \log p = 0$. We assume $P_{\nabla I}(x) > 0 \Rightarrow P_{\nabla J}(x) > 0$, since our model of the HVS smoothes $P_{\nabla I}(x)$.

3.2. Modeling Uncertainties in the Human Visual System

Any visualization on any display device is ultimately processed by the HVS and therefore subject to a multitude of additional adjustments and measurement inaccuracies, caused by the optical and sensory properties of the physical eye as well as by the neural circuitry after a signal was received from the photoreceptors. When photoreceptors detect a stimulus X , their response is effectively a random variable Y where the expected values of X and Y are proportional (within a certain range), but Y is subject to noise [Bia87]. The variable Y is said to *fluctuate* as described by a probability distribution $P(Y|X)$ for a stimulus X , while $\mathbb{E}(Y) \propto \mathbb{E}(X)$. We are concerned with stimuli X due to visualization images I , which we want to observe (with minimal loss) through the variable Y realized by the computation of our model output image J .

In order to compute our perception loss $L(I)$ for a displayed image I , we model three particular effects as a sequence of image operations on I resulting in the model output image J : Visual masking, sensor sensitivity, and local adaptation. Systems of similar form have been built to detect perceived image differences [Dal92], salient regions [FRC10], or visual masking [RPG99]. Fig. 2 provides an overview of our simulation of the HVS: Given an input

image I , we first model visual masking (loss of information due to, e.g., visual clutter) by applying Threshold Maps [RPG99]. Thus we obtain a distribution $P_m(J_m|I)$ of images J_m with tolerated error such that they are perceptually indistinguishable from I . Analogously, we model inaccuracy due to limited photoreceptor sensor sensitivity by a distribution $P_s(J_s|I)$. The resulting distribution of images registered by the HVS is furthermore subject to local adaptation to variance [BMD08] which we apply to realizations of the added uncertainties. The relative entropy of the resulting model output J with respect to the input image I provides the perception loss $L(I)$.

Design Choices While our perceptual model only considers parts of the complex HVS, we demonstrate that the simplicity of our proposed system based on image operations allows good reasoning about important boundary cases for robust optimization (Sect. 3.2.5), such as the preservation of interesting areas while penalizing regions with little information. We omit advanced visual attention or saliency modeling [BI13] concerned with selection mechanisms and a notion of relevance of visual information to the human brain. Thus, our model optimizes for concentrated studying of visualization images more than for perception at a glance. However, deployment of attention may strongly depend on task demands [TBHS03] while we aim for wider applicability.

3.2.1. Visual Masking by Threshold Maps

An important goal of visualization is the minimization of visual clutter: A high density of high-frequency detail makes it difficult to discern visual features and structures. This phenomenon of uncertainty due to visual masking has been modeled by Threshold Maps [RPG99], predicting the maximum luminance error for every pixel a human observer can tolerate. Threshold Maps build on three characteristics of the human visual system: Threshold sensitivity, defining the smallest noticeable luminance difference on a given background; contrast sensitivity, defining varying sensitivity depending on spatial frequencies in an image; and finally, contrast masking which elevates the threshold of luminance sensitivity non-linearly in response to certain contrast patterns. For their screen model, we assume faithful linear reproduction (i.e. a gamma-corrected display), given the maximum LCD brightness in cd/m^2 and the contrast ratio of the screen. Threshold Maps can be computed in real-time and naturally fit into our model of perceptual uncertainty: We use their predicted distribution $P_m(J_m|I)$ of perceptually indistinguishable images to model the corresponding perceptual uncertainty and steer our optimization away from visual clutter.

3.2.2. Sensor Sensitivity by Just Noticeable Differences

In order to account for the sensitivity limits of photoreceptive cells, we follow the common practice of modeling sensor noise [Bia87]. Human perception adapts to the intensity of stimuli to increase the dynamic range of signals that can be registered. As a consequence, the *just noticeable difference* (JND) in luminance, which is barely distinguishable above sensor noise, is a function of adaptation luminance. We compute it based on the contrast sensitivity function (CSF) of human perception by Barten [Bar89] (as also used internally by Threshold Maps [RPG99]): The JND in luminance is the contrast threshold obtained as the CSF's reciprocal, evaluated for an adaptation luminance and the spatial frequency of a

single pixel. We compute adaptation luminances in a 1° -diameter solid angle [RPG99, LRP97] where contrast sensitivity is maximal, yielding a conservative estimate. Like for Threshold Maps, a distribution $P_s(J_s|I)$ corresponding to sensor noise, and realizations thereof, are then easily obtained from uniform noise scaled to the JND.

Tristimulus Sensitivity We extend the JND in our model from luminance to color differences. The CIELAB color space was designed for matching color distances with perceived color differences. For each pixel, we construct a sphere around its CIELAB color coordinates such that the radius corresponds to the JND we computed based on adaption luminance. We then convert to the linear CIEXYZ space and thus obtain an anisotropic probability distribution for colored JND noise. Please refer to the supplemental for our derivation.

3.2.3. Local Contrast by Local Adaptation

Larger flat areas in visualization images require additional work by the HVS to discern subtle color differences which we want to minimize. Garvert and Gollisch [GG13] analyze how two kinds of local adaptation occur within the receptive field of ganglion cells which process visual information in the retina: First, adjustment to the local mean brightness, which we already covered by the JND. Second, adjustment to the variance of encountered stimuli. The mean and variance of stimuli in the receptive field fully characterize this effect [BMD08]. We model the latter adaptation by a variance normalization filter applied to the output J_{s+m} of the preceding steps of our model, i.e. $P_{m+s}(J_{m+s}|I) = P_m(\cdot|I) * P_s(\cdot|I)$. We compute the mean μ_g and variance σ_g^2 within the receptive field of a fictive ganglion cell g and obtain the final values $J(j)$ of our model by a mean-preserving contrast enhancement:

$$J(j) = \frac{J_{s+m}(j) - \mu_g(j)}{\sigma_g(j)} + \mu_g(j). \quad (3)$$

This operation is applied in LMS color space where the tristimulus values represent the receptor responses of the three types of cones in the human eye. The local adaptation parameters $\sigma_g^2(j), \mu_g(j)$ are estimated using a Gaussian weighting kernel while sampling the neighborhood around each pixel j . This is motivated by Enroth-Cugell and Robson [ECR66] who arrive at a Gaussian function when tracing the receptive field of a ganglion cell by measuring the sensitivity falloff. We set the standard deviation of this Gaussian field, based on the peak contrast sensitivity of HVS, to a 1° -diameter as in the previous section.

3.2.4. Model Output Images and Distribution

The distribution $P(J|I)$ of model output images J resulting from our full model of uncertainty in the HVS for a visualization image I is:

$$P(J|I) = \sigma_g^{-1} [P_m(\cdot|I) * P_s(\cdot|I)] (\sigma_g(J - \mu_g) + \mu_g). \quad (4)$$

Any particular model output image J obtained from the visualization image I after evaluating Eq. (3) is a realization of this distribution $P(J|I)$. In our implementation, we first compute the images J_m and J_s with scaled per-pixel-noise (Sect. 3.2.1 and 3.2.2) and add them both to the input I . After, we perform the local adaptation (Sect. 3.2.3) on the result. From this result J and the original input I

we get the quantitative metric by computing the Kullback-Leibler divergence (Sect. 3.1).

3.2.5. Model Quality and Pathological Example Cases

Our perception model considers a simplified subset of the complex processes in the HVS. Particularly, adaptation to variance is a complicated mechanism for which specific linear-nonlinear models have been built [BMD08, GG13]. However, the choice of our simple image processing steps works in our favor when reasoning about the overall behavior of the derived perception loss. Based on the analysis of a few pathological example cases of display images I as shown in Fig. 3, it becomes easy to grasp how the image transformations work together in a way that penalizes plain, low-contrast image areas, while detecting and preserving structural information in varying and high-contrast areas. In the shown model output images J we can see that uniformly colored areas are turned into noise (left column), resulting in large perception losses $L(I)$. The sensor sensitivity noise and the local variance adaptation work together to identify regions with low information content. For white noise inputs, the loss is driven by visual masking and local adaptation. Checker patterns with varying frequency, transition from a domination of masking in the high-frequency image areas to variance adaptation in the lower-frequency areas. Finally, a real-world example (right column) demonstrates all transformations working together to retain and thus reward structured, shaded input areas over unshaded input.

3.3. Automatic Parameter Selection and Optimization

In order to obtain good visualizations from complex, parameterized visualization techniques, we look for a configuration of parameters ρ that minimizes the perception loss $L(I)$. To drive the search for good configurations of optimized parameters ρ_o based on our loss function $L(I)$, we build on the online auto-tuning algorithm proposed by Tillmann et al. [TPKT16] and extensions to support discontinuous behavior changes [PTWT17] in our optimized visualization techniques (Sect. 3.3.1). To retain maximum user control where necessary, we partition the set of parameters ρ controlled by our method into free, automatically optimized parameters ρ_o , user-controlled parameters ρ_u , and model calibration parameters ρ_m .

Model Parameters ρ_m need to be predefined, so that our model of perception loss works as intended. For this, the specifications of the screen and work environment need to be configured, namely the screen's resolution and viewing distance as cycles per degree [RPG99], and the screen's contrast ratio and maximum brightness in cd/m^2 [Bar89]. We assume these parameters to be (roughly) constant for a once established work environment.

Optimized Parameters ρ_o is a vector of every *visualization* parameter, that is updated by our optimization algorithm. Real-, integer-valued as well as nominal types are supported, as long as a valid domain is specified. Every parameter in ρ_o is initialized with a random value inside its respective parameter domain.

User Parameters ρ_u is a vector of every *visualization* parameter, that is still controlled by the user, e.g. the camera position. Sect. 3.3.2 discusses how the optimization is reacting to user-incited changes.

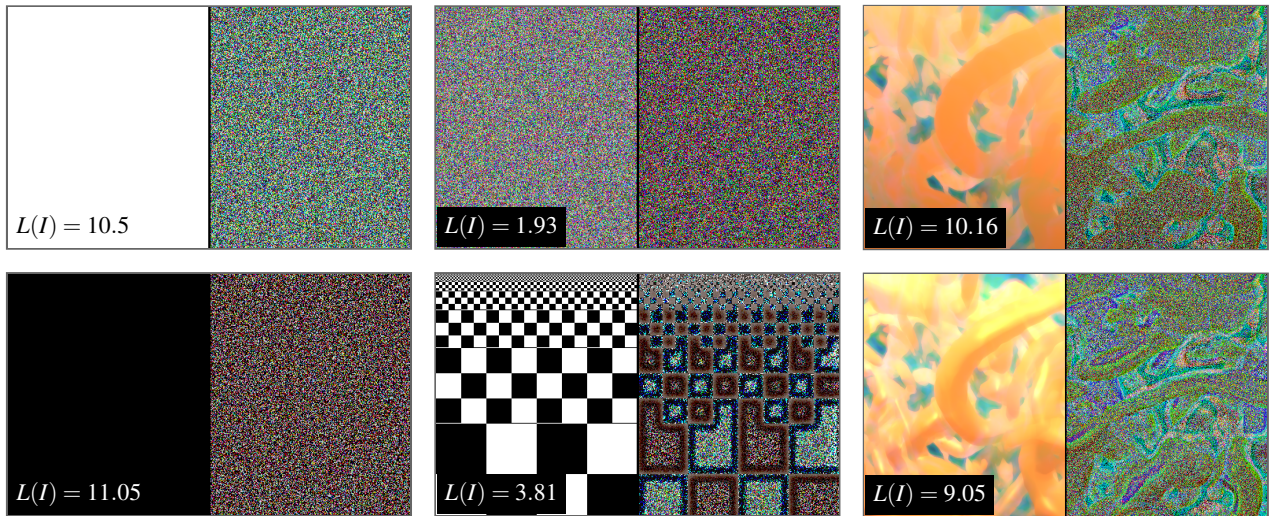


Figure 3: We show the results of the perceptual model in simple example cases (loss values, lower is better). Left (top and bottom): uniform colored regions are turned into noise and yield a high return of $L(I)$ because no features are present. Center top: noise is turned into noise and yields a low return for $L(I)$, which is in accordance with our model and information theory (uniform noise maximizes the entropy in an image). Center bottom: small checker patterns in the top cause visual masking and are consequently turned into noise; the score of $L(I)$ is better than in the uniform color cases because edges are recognized as features. Right: not shaded vs. shaded; the values of $L(I)$ suggest that the shaded version yields more features and improves perception.

3.3.1. Optimization Algorithm

We use the auto-tuner proposed by Tillmann et al. and Pfaffe et al. as our parameter search. Their work focuses on tuning performance parameters for the optimization of acceleration structure building heuristics for ray casting [TPKT16] and automated choice among several algorithms [PTWT17] for improved runtime. The approach is based on the Nelder-Mead search algorithm [NM65], a heuristic search that iteratively tightens the nodes of a simplex in parameter space around the predicted optimum. For each iteration, the search algorithm proposes a set of values for the parameters ρ_o to be explored. We pass these parameters to the visualization technique to obtain a corresponding tentative display image I , and subsequently compute a model output image J by realizing our model output distribution $P(J|I)$, passing the resulting loss $L(I)$ back into the search algorithm. Its convergence criterion is based on the size of the parameter-space simplex and is met once all simplex nodes fit in an ϵ -sphere around a predicted optimum. Note that multiple configurations may also lead to visually similar results for some visualization techniques (see Sect. 4).

The chosen search algorithm [TPKT16] converges quickly for a large class of cost or loss functions, although globally optimal results are not guaranteed. Due to a stochastic component in the search algorithm however, multiple trial runs can be used to enumerate multiple options. Although in general any parameter search algorithm could drive this optimization, our decision was determined by its fast convergence, robustness, and efficiency, causing low overhead on top of interactive visualization. Also, the variance introduced by the stochastic realizations in our model to compute the loss $L(I)$ is handled well, due to the auto-tuners' design to work with noisy in-

puts occurring in runtime measurements, which are naturally subject to fluctuation.

3.3.2. Online Parameter Optimization

For interactive exploratory sessions, we allow the algorithm to run in parallel to visualization after converging to suitable initial parameters. As user parameters ρ_u change during exploration (including virtual camera locations, light sources, as well as specific visualization technique parameters), we interactively re-optimize free parameters ρ_o to search for new, more suitable configurations.

Online Parameter Validation and Restart We continuously track the impact of user parameter changes on the perception loss $L(I)$: If parameter changes cause deterioration of the loss beyond a given threshold, we reset the optimization. We keep track of the best-scoring configuration before and after the restart to ensure good visualization quality. Listing 1 states the high-level online parameter optimization algorithm. We use $\alpha = 1.05$ to determine the threshold for restarting the parameter search.

Temporal Coherence Due to some of the heuristics used in the search algorithm, proposed parameter configurations may sometimes change erratically. We mitigate this issue in two ways: As shown in Listing 1, online re-optimization only ever applies new parameter configurations that score better than the previous configuration and we also maintain user control by manually pausing the optimization.

Parallel Optimization Our perceptual loss model is implemented in CUDA, which allows parallel computations in separate command streams. In order to minimize the overhead of online optimization,

Algorithm 1 Online Auto Tuning

```

1: loop ▷ score from last iteration
2:    $(params, converged) \leftarrow \text{tuner.next}(score)$ 
3:    $score \leftarrow \text{perception loss}(params)$ 
4:   if  $converged \wedge score > \alpha \cdot best$  then
5:     restart parameter search
6:   else if  $score < best$  then
7:      $best \leftarrow score$ 
8:      $\rho_o \leftarrow params$ 
9:   show  $(\rho_o \cup \rho_u)$  ▷ Always presents currently best

```

we run the optimization with low priority in parallel to the interactive visualization. Thus visualization stays responsive, while the computations required for image scoring can run fully asynchronously.

4. Results

In this section we will discuss the results for different scenarios in direct volume rendering, including the optimization of single and multiple parameters. In particular, we will show a parameter sensitivity analysis and the results of a user study supporting the validity of our model of perceptual loss. Finally, we will highlight a selection of applications outside direct volume rendering to prove the generality of our approach and show the limitations of the proposed technique in such contexts.

4.1. Setup

The model parameters ρ_m are the same for every setup. We assume a linear reproduction with common LCD brightnesses, i.e. around 300 cd/m^2 with a contrast ratio around $400 : 1$. The angular resolution of 94 pixels per degree was derived from a viewing distance of $0.8m$ to a 4K resolution 27 inch LCD monitor. To assess the accessibility of our method, tests were run on a modest workstation with an Intel Core i7 3.4 GHz CPU with 16 GB RAM, and an NVIDIA GTX 980Ti GPU. The image resolution matched the 4K screen.

Implementation We implemented a visualization framework in CUDA featuring volumetric rendering and streamlines, alongside our perceptual model since the computations mainly comprise image convolutions, per-pixel operations and histogram reductions, which are all suitable for massive parallelization on a GPU. Our model computations run asynchronously to the main visualization process, retaining stable real-time performance even in online optimization scenarios. Since our perceptual model is an image-space technique, our cost is independent of both the dataset size and the visualization technique cost, resulting in overhead only proportional to the screen resolution. Even when using a modest setup to perform visualization tasks, we can present an image rendered by a converged set of parameters after three to four seconds.

4.2. Loss Landscape and Efficacy for Volume Rendering

In the following, we look at the visualization results and the corresponding parameters chosen by our method in the context of direct

volume rendering. A particular challenge is posed by multiple parameters with similar impact in parts of the parameter domain, such as optimizing the intensity of multiple light sources simultaneously. Our volume renderer implements emission-absorption along with the Phong illumination model and includes low-pass filtered volumetric shadows (LPFVSs) as described by Ament et al. [ASDW14]. LPFVS is an efficient technique that improves the readability of direct volume rendering visualizations by controlling the softness of shadows, such that the directly visible structures are less impacted by visual masking due to high-frequency shadows. The softness of shadows is controlled by a cone angle parameter inside which light visibility is filtered for each point in the volume. The diffuse and specular albedo of the Phong illumination model are retrieved from the transfer function and multiplied with their respective global diffuse and specular coefficient when evaluated; the specular exponent is also globally configured for the whole dataset. In all experiments, initial parameter values were selected randomly in the range of their defined intervals, relieving the user of the cognitive load required for setting them up.

4.2.1. Indirect Shadow and Contrast Optimization

The LPFVS technique, which can improve contrast and shadows in direct volume rendering, is a good test case for the optimization efficacy for parameters with non-trivial optimal values. In Fig. 1, our method automatically reduces hard shadows that would cause visual masking and avoids dark or unlit regions. Simultaneously, we observe that the optimizer retains some structure in the shadow rather than trivially overblurring all shadow detail.

Robustness of Convergence for Multiple Parameters We test optimization efficacy for multiple free parameters with intertwined effect on the resulting images by adding material parameters and light intensity to be optimized alongside the cone angle. The Nelder-Mead search may get stuck in a local minimum of the perception loss $L(I)$, resulting in different viable solutions. We refer to Fig. 1 and Fig. 4 in the supplemental material for this section. We set up two experiments: in the first, we optimized cone angle, diffuse and specular reflectance, and the exponent of the Phong model; in the second, we also included the intensity of the light sources. All runs converge to useful parameter sets with slightly varying yet similar images and perceptual loss. We found that the optimizer’s performance drops particularly when many choices of ρ_o similarly influence the rendered image. On average, the algorithm converged after 47 iterations in the first experiment and 72 in the second. Encouragingly, the automatic selection of all five parameters ends with similar results as with hand-tuned light intensity.

Parameter Sensitivity We analyze the impact of optimized parameters on the loss function $L(I)$ by performing a parameter sensitivity analysis, computing variance-based sensitivity indices [SAA*10] S_i for the Vortex Cascade Dataset:

| | light | specular | diffuse | cone angle |
|-------|-------|----------|---------|------------|
| S_i | 0.28 | 0.21 | 0.18 | 0.11 |

Light source intensity has the highest impact, cone angle the lowest impact on our loss function $L(I)$. We can explain this by observing that adjusting only the cone angle at first reduces visual masking and later over-blurs the volumetric shadows; the remaining parameters,

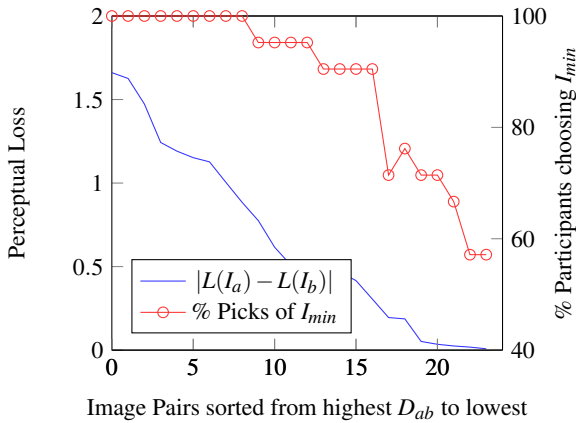


Figure 4: Shows the percentage of participants choosing the same better image as computed by our proposed perceptual loss metric. The image pairs have been sorted by decreasing difference in perceptual loss D_{ab} . With smaller D_{ab} the distribution of agreeing participants becomes more uniform.

instead, may cause drastic, global changes in the resulting image. For example, different configurations of the light source intensity may cause the image to be completely black or render the volume completely white.

4.2.2. Online Parameter Optimization

Fig. 8 in the supplemental material shows an image sequence showcasing the online parameter optimization in a scene containing a volumetric dataset and a single light source. The optimization selects the smoothing kernel size for volumetric soft shadows and a diffuse material coefficient. After an initial automatic parameter selection, the scene is rotated until the dataset is positioned between the light source and the view position, causing high-frequency patterns from shadows to overlay the colored structure of the surface. The subsequent increase in perception loss triggers a new parameter search, resulting in a newly optimized set of values. The complete process can also be seen in the supplemental video.

4.2.3. Other Applications in Volume Rendering

We showed the optimization of parameters concerned with lighting and shadows in volumes. On top of that, we applied our optimization method also to tuning a transfer function to a volume dataset as well as selecting interesting viewpoints. We describe these scenarios in the supplemental material.

4.3. User Study

We conducted a user study to empirically verify the validity of our model of the human visual system and perceptual loss metric. We deliberately chose the scenario to avoid manually dialing in rendering parameters and comparing resulting images as this process is complicated and tedious for study participants. Also, user-tuned parameter sets are generally not comparable, especially in scenarios where decreasing opacity or increasing light source intensity are

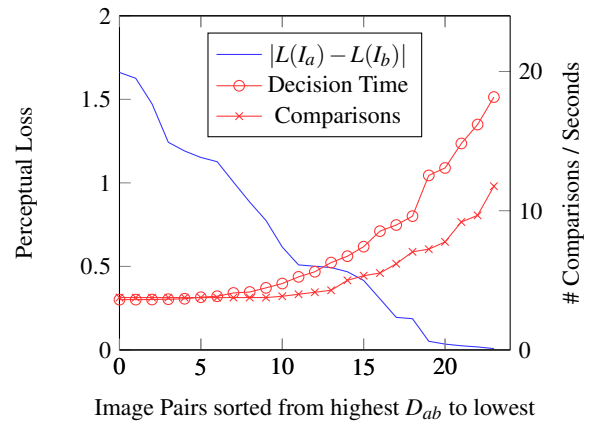


Figure 5: Shows the average time in seconds and the number of switching back and forth between images before a participant makes a decision on the better image. The image pairs have been sorted by decreasing difference in perceptual loss D_{ab} . With smaller D_{ab} , participants spent more time and the number of comparisons indicates the higher insecurity in their decision.

investigated, and would introduce significant complexity to the study evaluation. Moreover, acquiring a meaningful number of data points for the variety introduced in such a case would require the total number of participants to increase significantly, which is out of the scope of this work. We, therefore, chose a simple AB testing of 24 image pairs with 21 participants with normal or corrected to normal vision in a controlled environment with consistent room illumination and a calibrated monitor. The image pairs (I_a, I_b) were taken from a pool of pre-rendered images of the vortex cascade with the same experimental setup as described in Sect. 4.2.1. The same set of image pairs is shown, however the order of pairs is randomly permuted for every participant. Only a single image is shown full screen at a time, and it is possible to switch back and forth between the two images of the current pair as often as needed. For every image pair, the participant has to decide on a winner, being defined in this context as:

- better recognizable geometric detail,
- better perception of spacial depth,
- less disturbing visual artifacts.

Except for three, all participants come from a scientific background. The field of expertise of 5 participants is computer graphics, while the remaining belong to chemistry, physics, and mechanical engineering in equal parts.

We examine image pairs using $D_{ab} = |L(I_a) - L(I_b)|$, the absolute difference in perceptual loss between image I_a and I_b . If D_{ab} is large, we expect a high consensus of participants voting for the same image $I_{min} = \min(L(I_a), L(I_b))$. This expectation is rooted in the fact that one image is very close and the other very far from the optimum, hence the *better* image should be an obvious choice for the participant. Conversely, if D_{ab} is comparatively small, the choice becomes less evident. The expectation, in this case, is a more uniform distribution of the participant's picks. During the study evaluation, we saw that a similar difference in loss between two images is invariant of their good or bad quality. Fig. 4 shows this

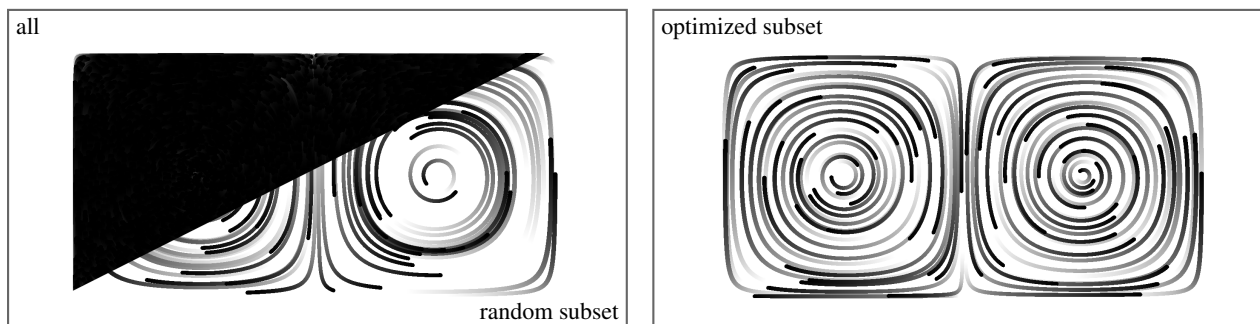


Figure 6: Automatic selection of streamlines with our optimization technique: we generated 1500 streamlines with the double gyre synthetic dataset. The left image is split in two: the upper left-hand side shows all streamlines unfiltered, while the lower right-hand side shows 80 streamlines selected with uniform random sampling. The right image instead shows a subset of 80 streamlines selected by our optimization.

correlation by plotting the quota of participants agreeing with the perceptual loss metric over D_{ab} . We can further support the claim of small D_{ab} resulting in difficult decisions in Fig. 5 showing that participants needed longer time and more switching back and forth between images until they made their decision. In 88.1% of the time, the participants chose I_{min} . When removing the 5% percentile of image pairs with the smallest D_{ab} , participants agreed 92.1% of the time, while with a 25% percentile removed the agreement raised to 95.2%. The combined results of this study, lead us to conclude that our metric $L(I)$ can reliably predict the decision of a human observer in this experimental setup.

4.4. Extension to other Visualization Problems

We also applied our model and optimization to other scenarios, i.e. tuning for specialized output devices and streamline selection. Given the generality of our approach and simple integration into existing visualization pipelines, we show that it can be applied to such scenarios, when tailored techniques are not available or required.

4.4.1. Colorimetric Characteristics of Displays

Any imaging device can be characterized by a transformation from the device color space (usually RGB) into one that describes the perceived color (CIEXYZ or CIELAB) and vice-versa. Moreover, incorporating different tone reproduction curves calibrated to the device in use is straightforward. Since our model requires only the CIELAB format as input, we can specifically optimize the visualization result to any display device. For example, we could tailor the visualization to a standard LCD, specifically calibrated displays for medical applications, or different viewing conditions (office vs. outdoor). Images showing the difference between applying the tone reproduction curve before and after optimization can be seen in Fig. 7 of the supplemental material.

4.4.2. Streamline Selection

We can construct a similar scenario as presented in Pineo and Ware [PW12] to select streamlines from a set of previously generated streamlines. Our optimization problem is defined as a selection from a boolean vector that represents whether a streamline is shown

or not. We can observe that the optimization quickly arrives at a point where the number of streamlines is roughly decided. Due to the abundance of local minima, configuration oscillate, leading to an unstable image. Therefore, we opt to terminate the optimization after the number of selected streamlines and $L(I)$ is stable enough, see Fig. 6. This suggests that our model $L(I)$ can be applied to other visualization problems and adapted to handle massive amounts of binary parameters. Note that compared to the neural network approach in [PW12], our method further allows for shading optimization and seamless use on 3D streamlines datasets.

5. Conclusion and Future Work

We introduced a model and a corresponding metric to estimate the loss of perceived information in (visualization) images accounting for visual masking, sensor sensitivity, and local adaptation of the human visual system. We laid the foundations for how this metric can be used to infer optimized parameter configurations for visualizations such that the perception of essential features is improved. Also the models' ability to generalize to different visualization problems and other applications, e.g. flow or information visualization with many more parameters, was demonstrated. The image based nature makes this model especially easy to integrate into existing rendering pipelines. It would be interesting to pursue a more sophisticated perceptual model. A model including color perception could further improve visual loss predictions for the parameter search and therefore the quality of visualization results. With spatio-temporal features and visual attention modeling one could adapt our approach to improve visualizations of time dependent datasets.

References

- [ASDW14] AMENT M., SADLO F., DACHSBACHER C., WEISKOPF D.: Low-pass filtered volumetric shadows. *IEEE Transactions on Visualization and Computer Graphics* 20, 12 (Dec 2014), 2437–2446. 1, 7
- [Bar89] BARTEN P. G. J.: The square root integral (sqri): A new metric to describe the effect of various display parameters on perceived image quality. In *Proc. Human Vision, Visual Processing, and Digital Display* (1989), vol. 1077. 4, 5
- [BBK*18] BEHRISCH M., BLUMENSCHNEIN M., KIM N. W., SHAO L., EL-ASSADY M., FUCHS J., SEEBACHER D., DIEHL A., BRANDES U., PFISTER H., SCHRECK T., WEISKOPF D., KEIM D. A.: Quality metrics for information visualization, 2018. 2

- [BCFW08] BARTZ D., CUNNINGHAM D., FISCHER J., WALLRAVEN C.: The Role of Perception for Computer Graphics. In *Eurographics 2008 - State of the Art Reports* (2008), Theoharis T., Dutre P., (Eds.), The Eurographics Association. 2
- [BI13] BORJI A., ITTI L.: State-of-the-art in visual attention modeling. *IEEE Transactions on Pattern Analysis and Machine Intelligence* 35, 1 (Jan 2013), 185–207. 4
- [Bia87] BIALEK W.: Physical limits to sensation and perception. *Annual review of biophysics and biophysical chemistry* 16, 1 (1987), 455–478. 4
- [BM10] BRUCKNER S., MÖLLER T.: Result-driven exploration of simulation parameter spaces for visual effects design. *IEEE Transactions on Visualization and Computer Graphics* 16, 6 (2010), 1468–1476. 3
- [BMD08] BEAUDOIN D. L., MANOOKIN M. B., DEMB J. B.: Distinct expressions of contrast gain control in parallel synaptic pathways converging on a retinal ganglion cell. *The Journal of Physiology* 586, 22 (2008), 5487–5502. 4, 5
- [BRB*13] BRAMON R., RUIZ M., BARDERA A., BOADA I., FEIXAS M., SBERT M.: An information-theoretic observation channel for volume visualization. *Computer Graphics Forum* 32, 3pt4 (2013), 411–420. 2
- [cDSK*14] Ç. DEMIRALP, SCHEIDEGGER C. E., KINDLMANN G. L., LAIDLAW D. H., HEER J.: Visual embedding: A model for visualization. *IEEE Computer Graphics and Applications* 34, 1 (Jan 2014), 10–15. 2
- [daEMdA04] DE ALBUQUERQUE M. P., ESQUEF I., MELLO A. G., DE ALBUQUERQUE M. P.: Image thresholding using tsallis entropy. *Pattern Recognition Letters* 25, 9 (2004), 1059 – 1065. 2
- [Dal92] DALY S. J.: Visible differences predictor: an algorithm for the assessment of image fidelity. In *Proc. Human Vision, Visual Processing, and Digital Display III* (1992), vol. 1666, pp. 1666 – 1666 – 14. 2, 4
- [ECR66] ENROTH-CUGELL C., ROBSON J. G.: The contrast sensitivity of retinal ganglion cells of the cat. *The Journal of Physiology* 187, 3 (1966), 517–552. 5
- [FI08] FURUYA S., ITOH T.: A streamline selection technique for integrated scalar and vector visualization. *VIS 08. IEEE Visualization, Poster Session* 2, 4 (2008). 2
- [FRC10] FRINTROP S., ROME E., CHRISTENSEN H. I.: Computational visual attention systems and their cognitive foundations: A survey. *ACM Transactions on Applied Perception* 7, 1 (Jan. 2010), 6:1–6:39. 4
- [GG13] GARVERT M., GOLLISCH T.: Local and global contrast adaptation in retinal ganglion cells. *Neuron* 77, 5 (2013), 915 – 928. 5
- [HE12] HEALEY C., ENNS J.: Attention and visual memory in visualization and computer graphics. *IEEE Transactions on Visualization and Computer Graphics* 18, 7 (July 2012), 1170–1188. 2
- [JAS89] JOHN A. SAGHRI PATRICK S. CHEATHAM A. H.: Image quality measure based on a human visual system model. *Optical Engineering* 28 (1989), 28 – 28 – 6. 2
- [JC10] JÄNICKE H., CHEN M.: A salience-based quality metric for visualization. *Computer Graphics Forum* 29, 3 (2010), 1183–1192. 2
- [JM04] JEON J., MANMATHA R.: Using maximum entropy for automatic image annotation. In *Image and Video Retrieval* (Berlin, Heidelberg, 2004), Enser P., Kompatsiaris Y., O'Connor N. E., Smeaton A. F., Smeulders A. W. M., (Eds.), Springer Berlin Heidelberg, pp. 24–32. 2
- [KL51] KULLBACK S., LEIBLER R. A.: On information and sufficiency. *The Annals of Mathematical Statistics* 22, 1 (1951), 79–86. 4
- [KON02] KEYSERS D., OCH F. J., NEY H.: Maximum entropy and gaussian models for image object recognition. In *Pattern Recognition* (Berlin, Heidelberg, 2002), Van Gool L., (Ed.), Springer Berlin Heidelberg, pp. 498–506. 2
- [Lar16] LARKIN K. G.: Reflections on shannon information: In search of a natural information-entropy for images. *CoRR abs/1609.01117* (2016). 3
- [LBH12] LINDOW N., BAUM D., HEGE H.-C.: Perceptually linear parameter variations. *Computer Graphics Forum* 31, 2pt3 (2012), 535–544. 2
- [LJ11] LIN W., JAY KUO C.-C.: Perceptual visual quality metrics: A survey. *Journal of Visual Communication and Image Representation* 22, 4 (2011), 297–312. 2
- [LRP97] LARSON G. W., RUSHMEIER H., PIATKO C.: A visibility matching tone reproduction operator for high dynamic range scenes. *IEEE Transactions on Visualization and Computer Graphics* 3, 4 (Oct 1997), 291–306. 5
- [LSP05] LAZEBNIK S., SCHMID C., PONCE J.: A maximum entropy framework for part-based texture and object recognition. In *null* (2005), IEEE, pp. 832–838. 2
- [Lub95] LUBIN J.: *A Visual Discrimination Model for Imaging System Design and Evaluation*. World Scientific, 1995, pp. 245–283. 2
- [MCHM10] MARCHESIN S., CHEN C., HO C., MA K.: View-dependent streamlines for 3d vector fields. *IEEE Transactions on Visualization and Computer Graphics* 16, 6 (Nov 2010), 1578–1586. 2
- [MMGB17] MINDEK P., MISTELBAUER G., GRÖLLER E., BRUCKNER S.: Data-sensitive visual navigation. In *Proceedings of the 33rd Spring Conference on Computer Graphics* (New York, NY, USA, 2017), SCCG '17, ACM, pp. 9:1–9:10. 3
- [NM65] NELDER J. A., MEAD R.: A Simplex Method for Function Minimization. *The Computer Journal* 7, 4 (01 1965), 308–313. 6
- [PTWT17] PFAFFE P., TILLMANN M., WALTER S., TICHY W. F.: Online-autotuning in the presence of algorithmic choice. In *2017 IEEE International Parallel and Distributed Processing Symposium Workshops (IPDPSW)* (2017), IEEE, pp. 1379–1388. 5, 6
- [PW12] PINEO D., WARE C.: Data visualization optimization via computational modeling of perception. *IEEE Transactions on Visualization and Computer Graphics* 18, 2 (Feb 2012), 309–320. 3, 9
- [RPG99] RAMASUBRAMANIAN M., PATTANAIK S. N., GREENBERG D. P.: A perceptually based physical error metric for realistic image synthesis. In *Proc. ACM SIGGRAPH* (New York, NY, USA, 1999), SIGGRAPH '99, ACM Press/Addison-Wesley Publishing Co., pp. 73–82. 2, 3, 4, 5
- [SAA*10] SALTELLI A., ANNONI P., AZZINI I., CAMPOLONGO F., RATTO M., TARANTOLA S.: Variance based sensitivity analysis of model output. design and estimator for the total sensitivity index. *Computer Physics Communications* 181, 2 (2010), 259 – 270. 7
- [TBHS03] TRIESCH J., BALLARD D. H., HAYHOE M. M., SULLIVAN B. T.: What you see is what you need. *Journal of Vision* 3, 1 (02 2003), 9–9. 4
- [TM04] TORY M., MOLLER T.: Human factors in visualization research. *IEEE Transactions on Visualization and Computer Graphics* 10, 1 (Jan 2004), 72–84. 2
- [TMWS13] TAO J., MA J., WANG C., SHENE C.: A unified approach to streamline selection and viewpoint selection for 3d flow visualization. *IEEE Transactions on Visualization and Computer Graphics* 19, 3 (March 2013), 393–406. 2
- [TPKT16] TILLMANN M., PFAFFE P., KAAG C., TICHY W. F.: Online-autotuning of parallel sah kd-trees. In *2016 IEEE International Parallel and Distributed Processing Symposium (IPDPS)* (2016), IEEE, pp. 628–637. 5, 6
- [TTL03] TAO W.-B., TIAN J.-W., LIU J.: Image segmentation by three-level thresholding based on maximum fuzzy entropy and genetic algorithm. *Pattern Recognition Letters* 24, 16 (2003), 3069 – 3078. 2
- [WS11] WANG C., SHEN H.-W.: Information theory in scientific visualization. *Entropy* 13, 1 (2011), 254–273. 2
- [XLS10] XU L., LEE T., SHEN H.: An information-theoretic framework for flow visualization. *IEEE Transactions on Visualization and Computer Graphics* 16, 6 (Nov 2010), 1216–1224. 2